Structural Dynamics of Lipid Bilayer Membranes Explored by Magnetic Field Effect Based Fluorescence Microscopy

Sakurai, Manabu
Kobori, Yasuhiro
Tachikawa, Takashi

Structural Dynamics of Lipid Bilayer Membranes Explored by Magnetic Field Effect-Based Fluorescence Microscopy

Manabu Sakurai[†], *Yasuhiro Kobori*[†,‡] *and Takashi Tachikawa*[*,†,‡]

[†] Department of Chemistry, Graduate School of Science, Kobe University, 1-1 Rokkodai-cho, Nada-ku, Kobe, 657-8501, Japan

[‡] Molecular Photoscience Research Center, Kobe University, 1-1 Rokkodai-cho, Nada-ku, Kobe, 657-8501, Japan

ABSTRACT

Lipid bilayer membranes are known to exist as heterogeneous and dynamic structures where the molecules are always moving and fluctuating under physiological conditions. Magnetic field effects (MFEs) studied herein are phenomena in which the exciplex emission from an electron donor-acceptor dyad increases or decreases by applying an external magnetic field. The characteristic dependence of MFEs on the viscosity and polarity of the surrounding medium has been applied to investigate the local environments around the probe molecule. In

this study, a novel MFE-based fluorescence microscopy technique was developed to explore the structural dynamics of lipid bilayer membranes. The vesicle formation during the membrane deformation was selectively visualized through the MFEs, thus allowing the extraction of information on the cellular dynamics at high temporal and spatial resolutions. This highly versatile and powerful technique is applicable to a wide range of areas, such as biology and materials science.

1. INTRODUCTION

The local elastic properties and structures of lipid bilayer membranes are closely related to cellular dynamics such as nucleocytoplasmic transport, endocytosis, and metabolism.[1,2] The dynamic structural changes of lipid membranes and liposomes have been thus studied by various methods.[3–7] For instance, the diffusion of single-molecule lipids was reported to be affected by membrane curvature where highly confined motion was observed with fluorescence techniques.[3] It was suggested that such curved regions of deformed membranes play a significant role in lipid sorting and protein interactions in cells.[2] To model the deformation process, the lipid bilayer was destroyed by adding surfactants or organic solvents, such as acetonitrile and ethanol.[4,5,8] The additives are also known to metabolize intracellularly to produce toxic cyanide and the like, which adversely affect the cell viability.[9,10] However, structural features and dynamics of membranes were only inferred from visual information obtained most commonly from optical images. In addition, the so-called micropolarity is an important factor that determines the degree of electrostatic interaction between biomolecules,[11,12] and it is closely related to protein interactions and formation of biopolymers.[13] Hence, the measurement technique that acquires

information on the polarity and viscosity in the local environments such as curved regions is indispensable for elucidating the detailed structural and mechanical properties of biological materials.

Fluorescence microscopy is an important technique for observing tissues, cells, and other microscopic matters including inorganic materials.[14] Recent developments of microscopic techniques with designed fluorescent probes have found a wide range of applications such as localization of proteins, visualization of specific interactions, and dynamic analysis of signaling molecule.[11,15–19] For instance, coumarin derivatives have been used to monitor micropolarity in biological systems because its fluorescence wavelength depends on the polarity of the solvent.[17] The change of the dielectric gradient in the lipid bilayer membrane during the phase transition has also been reported using the probes such as 6-propionyl-2-(dimethyl-amino)naphthalene (Prodan).[19] Yui et al. also proposed a technique for evaluating microviscosity from fluorescence lifetime by applying the property that the viscosity affects the nonradiative deactivation via intramolecular rotation of 8-anilinonaphthalene-1-sulfonate (ANS) in the excited state.[18]

The magnetic field effect (MFE) on photoinduced electron transfer reactions is a spin-dependent phenomenon that changes the reaction rates and yields by applying a weak external magnetic field (less than 100 mT).[20–29] This type of MFE is theoretically established in the framework of the so-called radical pair mechanism.[30–34] The MFEs studied here are caused by indirectly altering the population of charge-separated radical ion pair (RIP) state in equilibrium with the exciplex,[23–25,35,36] which results in an increase or decrease in the intensity of the exciplex emission (Figure 1a). Specifically, an excited acceptor molecule that is generated by light irradiation forms a singlet RIP by intramolecular electron transfer, followed by an intersystem crossing (ISC) to a triplet RIP by hyperfine interaction (HFI). When an external

magnetic field is applied, the degree of singlet (S)-triplet (T) mixing is reduced. This reduction occurs because the magnetic field breaks the degeneracy of the S and $T_{\pm}$ states by Zeeman splitting if the exchange interaction (*J*) is weak in the RIP, thereby reducing the number of the states accessible to spin mixing. As a result, the exciplex emission in equilibrium with the singlet RIP is enhanced. Furthermore, the characteristics of MFEs on this photochemical process depend on physical quantities such as polarity and viscosity.[20–22,25,27,29] Despite the usefulness and importance of MFEs, their applications in optical imaging have been very limited. Woodward et al. proposed an approach based on optical absorption microscopy to detect radical pairs formed from flavin adenine dinucleotide.[37,38] In a previous study of MFE-based fluorescence imaging, local magnetic fields created by ferromagnetic nanostructures were visualized.[39,40] However, there are no studies in which local environments and chemical reactivity in heterogeneous systems are visualized by applying the characteristics of MFEs.

In this study, we developed a strategy for characterizing dynamic structural changes of lipid bilayer membranes by monitoring the responses of exciplex emission to local environments and external magnetic fields with a magnetic-field-responsive probe (MAn-10-O-2-DMA) in which 9-methylanthracene (MAn) and *N*,*N*-dimethylaniline (DMA) are linked by a spacer (Figure 1b). By using the MFE-based fluorescence microscope developed herein, useful information related to the local polarity and molecular motion of transient states that occur during membrane deformation are obtained.

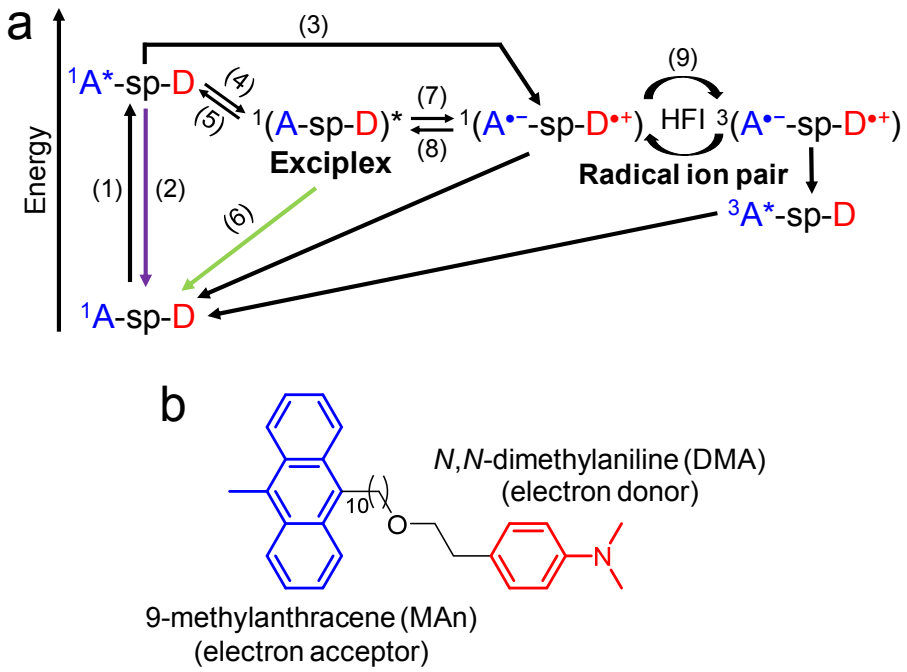

Figure 1. (a) Reaction scheme underlying MFEs on photoinduced electron transfer reaction in exciplex-forming electron donor (D)-acceptor (A) dyad system ("sp" indicates spacer). Processes include (1) photoexcitation, (2) fluorescence of A moiety, (3) formation of RIP by electron transfer, (4) formation of exciplex, (5) reversible interconversion of exciplex to locally excited state, (6) exciplex emission, (7) dissociation from exciplex to RIP, (8) exciplex formation from RIP, and (9) S-T conversion by HFI. Since phosphorescence process was not observed in all the experiments, it is omitted. (b) Molecular structure of magnetic-field-responsive probe employed in this study.

2. EXPERIMENTAL SECTION

Formation of Lipid Bilayer Membranes on Cover Glass. In a typical procedure for the preparation of lipid bilayer membranes,[41] 1.75 mg of 3-sn-phosphatidylcholine, from Egg Yolk, was dissolved in 5 mL of chloroform. MAn-10-O-2-DMA was then added to the solution ([MAn-10-O-2-DMA] = 0.1 mM). The chloroform was removed by distillation under reduced

pressure, and 5 mL of phosphate buffered saline (PBS) solution (10 mM, pH 7.6, NaCl 100 mM), which was prepared using phosphate buffer solution (Nacalai, 0.1 M, pH 7.6), NaCl (Nacalai, 99.5%), and Milli-Q water, was added, and the resultant mixture was sonicated for 30 minutes in ice bath. Subsequently, liposomes were prepared using a liposome preparation device (Avanti, Mini-Extruder) and polycarbonate filter (average pore diameter of 200 nm). The liposome solution was dropped on a clean cover glass (Matsunami Glass), left to stand at 60 °C for 1 hour, and then the cover glass was gently washed with PBS buffer to form a membrane film. In addition, the lipid bilayer membrane was destroyed by adding PBS solution containing acetonitrile (30 or 50 vol%) onto the cover glass in the chamber. Acetonitrile was used as received (Nacalai, >99.8%). For staining of lipid bilayer membranes, the membrane on the cover glass was incubated with approximately 10 μg ml^{-1} $DiOC_{14}(3)$, hydroxyethanesulfonate (PromoKine) in PBS solution. And then, the stained membrane was rinsed with PBS solution.

Instruments. The experimental setup was based on a Nikon Ti-E inverted wide-field fluorescence microscope. The 405-nm continuous wave laser (Coherent, OBIS 405LX) through an objective lens (Nikon, CFI Plan Apo λ 100×H; NA 1.45) was used to excite the sample. The emission images were recorded on an electron-multiplying charge-coupled device (EMCCD) camera (Photometrics, Evolve 512) using the open source microscopy software Micro-Manager (https://www.micro-manager.org/). A suitable dichroic mirror (Semrock, Di02-R405) and a longpass filter (Semrock, BLP01-458R or BLP01-405R) were used to improve the signal-to-noise ratio. For the spectroscopy, only the emission that passed through a slit entered the imaging spectrograph (SOL instruments, MS3504i) equipped with a CCD camera (Andor, DU416A-LDC-DD). The data were analyzed using the open source image software ImageJ (http://rsb.info.nih.gov/ij/) and Origin 2018 (OriginLab). All experimental data were obtained at

room temperature. A magnetic field of about 3 to 300 mT was applied by moving a neodymium magnet with a stepping motor (Thorlabs, NRT150). The magnetic fields at the sample position were measured by tesla-meter (Magna, MG-801). The absorption and fluorescence spectra were measured by a UV-visible spectrophotometer (JASCO, V-770) and a fluorescence spectrophotometer (JASCO, FP-8300), respectively.

Sample Preparation for MFE Measurements in Bulk Solvents. The synthesis procedures of the probe (MAn-10-O-2-DMA) are described in the Supporting Information (Figures S1-S6). MAn-10-O-2-DMA was dissolved in solvent, and the solution was bubbled with argon gas to remove dissolved oxygen. The samples for the microscope measurements were prepared in the glove box filled with argon gas.

Solvent Polarity Dependence of Exciplex Emission and MFEs. In order to obtain a calibration line, the dependence of exciplex emission and MFEs on solvent dielectric constant (ε_s) was evaluated for each solvent. MAn-10-O-2-DMA was dissolved in a mixed solvent of propyl acetate (PA, TCI >98.0%, ε_s = 6) and butyronitrile (BN, TCI >99%, ε_s = 24.7), and the MFEs and exciplex maximum wavelength were measured. The mixed solvents of PA and BN allow for a systematic variation of ε_s in the range from 6 to 24.7 at 295 K. The ε_s of the mixed solvent of PA and BN was determined using this equation $\varepsilon_s = w_{PA}\varepsilon_{PA} + (1 - w_{PA})\varepsilon_{BN}$.[42,43]

Confirmation of Exciplex Emission. In order to confirm the contribution of the excimer emission, MAn-10-O-2-DMA and MAn were introduced into the vesicles, and fluorescence measurements were performed. The samples were prepared in the following procedure. 1.75 mg of 3-sn-phosphatidylcholine, from Egg Yolk was dissolved in 5 mL of chloroform. After that, MAn-10-O-2-DMA or MAn was added so as to be 0.1 mM each. After the chloroform was

removed by distillation under reduced pressure, 5 mL of PBS solution (10 mM, pH 7.6, NaCl 100 mM) was added, and the mixture was sonicated for 30 minutes in ice bath.

3. RESULTS AND DISCUSSION

Optical and MFE Characteristics of MAn-10-O-2-DMA. The UV-visible absortpiton and fluorescence spectra of MAn-10-O-2-DMA in BN are shown in Figure 2a. In addition to the emission band due to the fluorescence from the locally excited state, the broad emission band with a peak at around 580 nm was obseved. As judged from the Lippert-Mataga plots (Figure S7),[44,45] i.e., the linear relationship between the energy of the exciplex emission maximum and solvent polarity parameter (Δf), this emission is attributed to the exciplex fluorescence, and further responds to the external magnetic field (see the red line Figure 2a and Figure S8). The strength of MFE (χ) is expressed by eq 1:

$$\chi(B) = ((I(B) - I(0))/I(0) \times 100 \quad (1)$$

where I (B) and I (0) are the exciplex emission intensity with and without the applied magnetic fields, respectively. The χ values for MAn-10-O-2-DMA in BN increased with increasing magnetic fields and reached a saturation value of approximately 15% at a magnetic field of approximately 30 mT (Figure S9). Moreover, the χ values exhibit obvious dependence on solvent polarity (Figure 2b). The solvent polarity dependence of χ can be explained in terms of changes in the free energy of the exciplex and RIP states.[25–27,29,46] The exciplex forms upon collision between the excited MAn and DMA or recombination of the RIP generated by electron transfer [process (4) or (8) in Figure 1a, respectively]. When the solvent polarity is low, the electron

transfer is drastically suppressed due to destabilization in the weakly coupled RIP state; this situation results in the preferred formation of an exciplex that is stabilized by both partial charge transfer and wavefunction overlap and minimizes MFEs because the exciplex emission does not pass through the RIP state in which the S-T conversion occurs.[29] Conversely, as the solvent polarity increases, the MFEs are enhanced due to the increased population of RIPs.

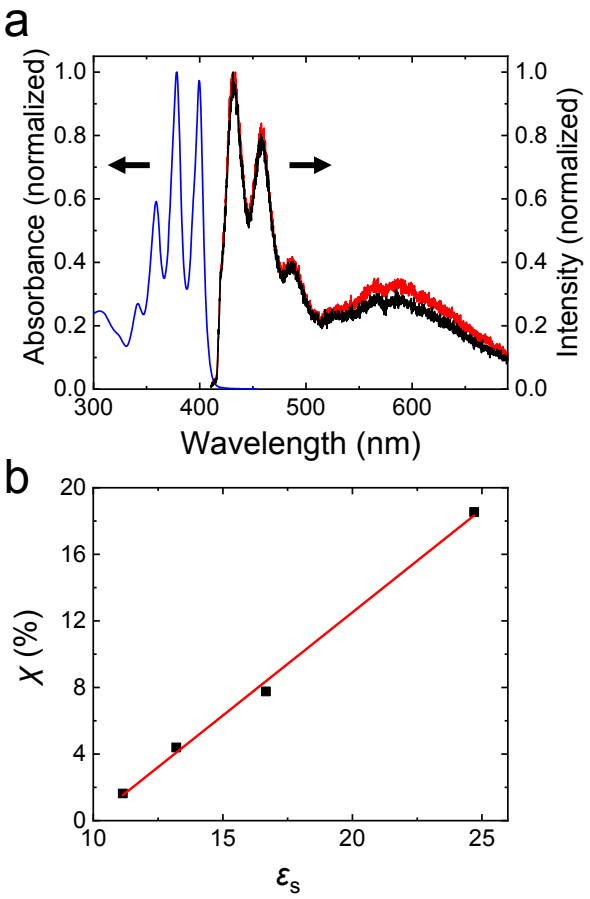

Figure 2. (a) UV-visible absorption (blue line) and fluorescence spectra of MAn-10-O-2-DMA in BN. Fluorescence spectra were measured with magnetic field (red line) and without magnetic field (black line) under a fluorescence microscope. The excitation wavelength was 405 nm. (b) Plots of the χ values against ε_s.

Fluorescence Imaging of Deformation Processes. Figure 3a shows a fluorescence image observed immediately after the preparation of lipid bilayer membranes containing the probe molecules and acetonitrile on the cover glass under 405-nm laser irradiation. The acetonitrile (30 vol% in Ar-saturated water) was added to induce the deformation of the membrane. For comparison, a fluorescence image of the sample without acetonitrile is given in Figure S10. In addition to the homogeneous membrane, the domains where lipids aggregated in the membrane, possibly due to coordination of acetonitrile to a hydrophilic part of the lipid, were visualized as bright spots. The bright spots become vesicles after a certain period of time and dissociate from the membrane surface (Figure S11). With increasing incubation time up to ca. 10 minutes, the lipids dissociated from the cover glass to form giant unilamellar vesicles with dimensions of tens of micrometers (Figures 3b,c and S12e,f). To summarize the above-mentioned information, the membrane deformation is illustrated in Figure 3d; the processes including fluctuation and dissociation correspond to those proposed by previous studies.[4,5]

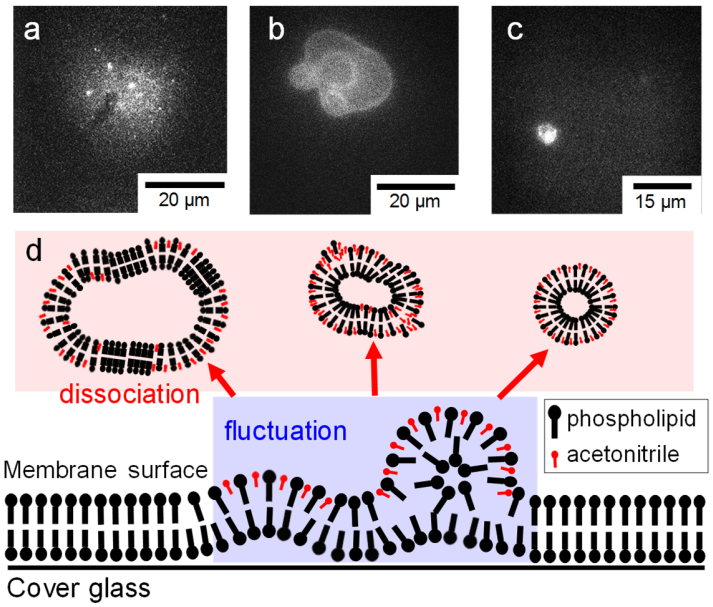

Figure 3. (a,b,c) Fluorescence images captured during lipid bilayer disruption processes. (d) Schematic diagram of membrane destruction process induced by addition of acetonitrile.

Micropolarity in the Deformed Membranes. As mentioned above, the peak wavelength of the exciplex emission depends on the solvent polarity according to the Lippert-Mataga equation.[44,45] The fluorescence spectra of each state (vesicle and membrane surface such as Figures 3a and b) before and after introducing acetonitrile were measured to evaluate the micropolarity in the deformed membranes using a calibration curve of the emission peak energies versus the solvent polarities (Figure S7). For example, an aggregate in Figure 3a shows the broad spectrum with a peak at about 540 nm, which is typical of the exciplex emission (Figure S13). The fluorescence spectrum was measured after MAn was introduced into the membrane, and no significant emission in the long wavelength region was observed (Figure S14). Therefore, the contribution of excimer emission is negligible in this wavelength region. The ε values determined at each state are summarized in Figure 4. Upon the addition of acetonitrile, the

emission peaks shifted to longer wavelengths, indicating that the local dielectric constant (ε) values increased by inclusion of acetonitrile into the hydrophilic regions of the lipid bilayers. A further discussion on the micropolarity is given in the Supporting Information.

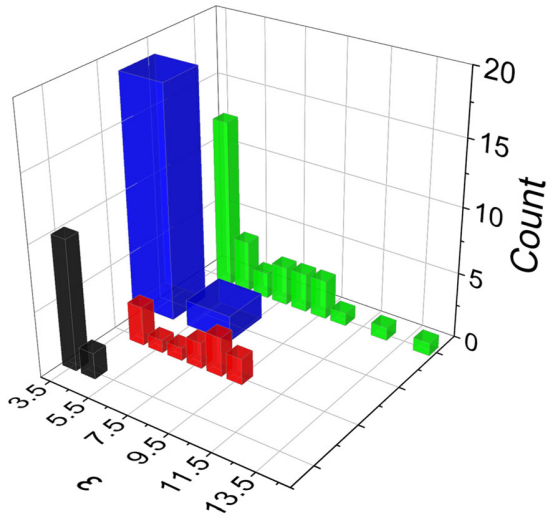

Figure 4. Distributions of local ε values obtained from emission peak wavelengths for each state. The bars were obtaiend for membrane surfaces before (black) and after (red) the addition of acetonitrile, vesicles dissociated from the membrane surface (blue), and domains where the lipids aggregate in the membrane (green).

MFE Imaging. By simultaneously examining the dependence of the emission intensity on the magnetic field, significant MFEs were observed for smaller vesicles. Figure 5a shows a typical MFE image that was reconstructed from maximum χ values calculated by eq 1 for each pixel of Figrue 3c (see the region enclosed in red line). The dependence of χ on external magnetic field over the vesicle is also shown in Figure 5b. The χ values varied from approximately 0% to 5% at different locations of the vesicle, suggestign the heterogeneous environments in the vesicle. In the regions with the highest χ value, the micropolarity was high

enough to solvate the RIPs that incorporated acetonitrile and water molecules, which resulted in the significant MFEs. However, in the regions where acetonitrile coordination was not sufficient, the MFEs were weak or absent because the RIPs hardly formed. This situation is similar to those in the membrane and vesicle (Figures 3a, b) where negligible MFEs were observed.

Interestingly, a certain degree of correlation was confirmed between the fluorescence intensity and the MFEs. The fluorescence intensities and corresponding MFEs along the solid and dotted blue lines are plotted at each pixel as shown in Figures 5c and d, respectively. In the region where MFE is high, the fluorescence intensity tends to be strong. Since the curvature of the membrane increases by addition of acetonitrile, the hydrophobic groups would have loose structures without ordered packing in the curved regions. Therefore, a number of probe molecules can readily move to such deformed regions, resulting in the increase of fluorescence intensity. The presence of acetonitrile leads to the increase of the local polarity, and the RIP is more likely to form, thus resulting in the MFEs.

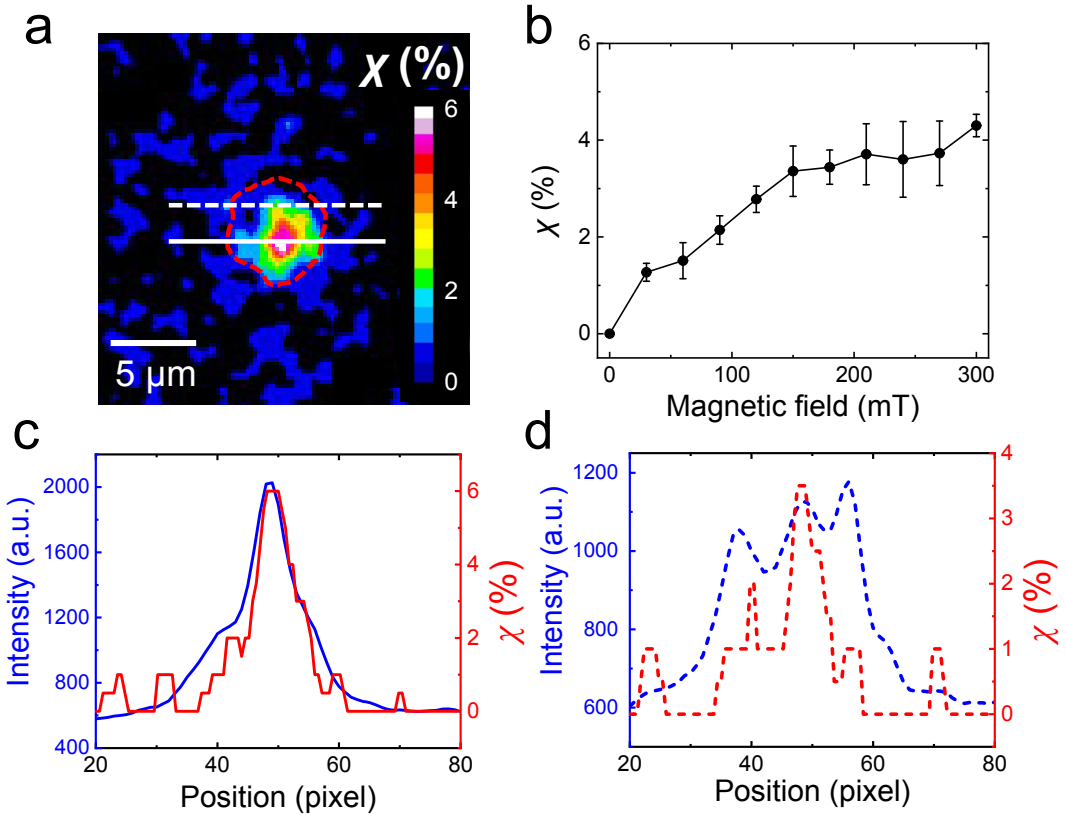

Figure 5. (a) Mapping of maximum χ values obtained in each pixel of 21.3 × 21.3 μm^2 area of Figure 3c. (b) Dependence of χ on external magnetic fields over the vesicle in panel a. (c,d) Plots of the fluorescence intensities (blue) and χ values (red) along the solid (c) and broken (d) lines in panel a, respectively.

MFE Measurements of Transient Species. To obtain dynamic information, we measured the temporal response of the emission intensity to magnetic field sweeps (3-300 mT) during incubation after adding acetonitrile (Figure 6a). As demonstrated in Figure 6b, the domain A shows only a fading due to photobleaching, while the domain B clearly exhibits MFEs in the initial time (0-5 s) and a subsequent sharp decrease of the emission intensity, possibly due to structual or environmental changes in the vesicle (Figures S15 and S16). The observed MFEs suggest that the polar environment around the probes is sufficient to solvate long-range RIPs by

the influx of acetonitrile, causing effecient S-T mixings. Such local membrane fluctuations may eventually lead to spontaneous motion,[47] as inferred from shape changes of the domain B (insets in Figure 6b) during the measurement, while the domain A kept its shape. Although there is uncertainty because of the laser-induced fading, χ value was tentatively estimated as approximately 7%. The absence of MFE in the domain A would be interpreted in terms of the exchange interaction as described later.

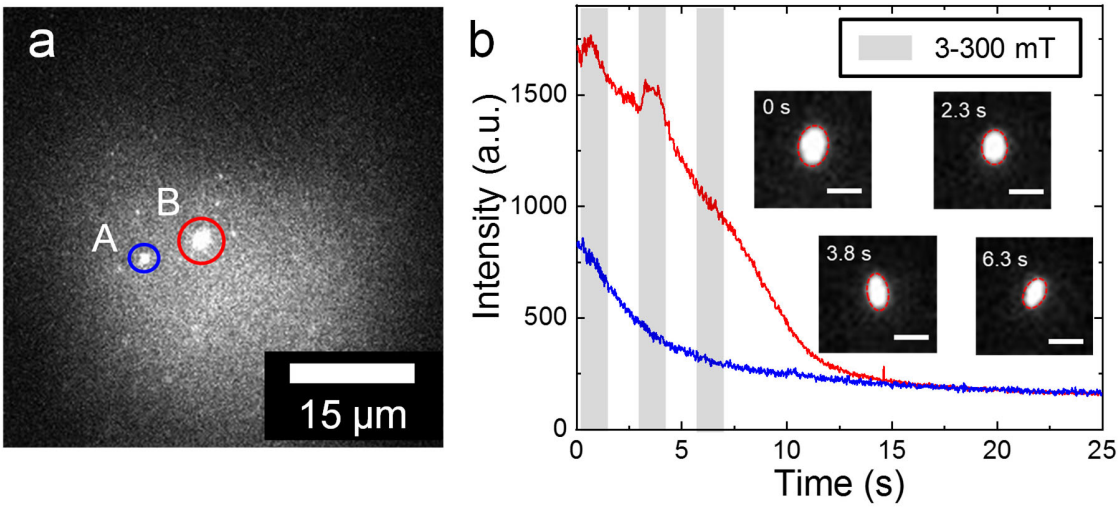

Figure 6. (a) Fluorescence image of domains where the lipids aggregate on the membrane surface. (b) The time traces of the emission intensity obtained for domains A (blue line) and B (red line) with and without magnetic field. The inset shows the shape of domain B at each time. The scale bars are 2 μm.

Effect of Exchange Interaction. In Figure 5b, χ reached a saturation value of approximately 3.5% at a magnetic field of about 150 mT, and the $B_{1/2}$ value obtained (i.e., the magnetic field at which the change in emission intensity reaches half of its saturation value) was 60 ± 10 mT. The $B_{1/2}$ value of MAn-10-O-2-DMA dissolved in neat BN was approximately 15

mT (Figure S9), whereas the reported value is 9.5 mT for the same molecule in BN, although the magnetic field effect on reaction yield (MARY) curves matched closely.[20,22,23] The main reasons for the underestimation (approximately 5 mT) in this experiment were the probe thickness (1.0 mm) of the Gauss meter and the backlash of the stepping motor. Even with this error, the $B_{1/2}$ value in the vesicles was significantly larger than those in the bulk solutions. The large increase in $B_{1/2}$ (as high as 60 mT) was possibly due to the fact that S-T dephasing, caused by the temporal variation of J, promoted the mixing of S and $T_{\pm}$ (Figure S17, Table S1). The influence of this type of mixing on the MARY has been reported by Maeda et al.[48] In addition, Hoang et al. recently reported that $B_{1/2}$ increases up to 38 mT when the chain length between the MAn and DMA moieties shortens; this increase was explained by an increase in S-T dephasing.[23] Such a large $B_{1/2}$ shift can adequately explain the system examined in this study. It was presumed that the observed MFEs originated from the solvation of the precursor RIP by acetonitrile, or the hydrophilic part of the lipid, or both. When acetonitrile is flowed into the membrane, the probe molecules prefer to be solvated in the hydrophilic region. As the solvation radius is reduced, the motion of the RIP state of the probe would be spatially restricted (Figure 7a). In other words, when it becomes impossible to stretch the alkyl chain, J increases. In addition, J varies significantly due to the repeated collision and separation of the RIPs within a restricted space, which results in a significant increase in $B_{1/2}$.

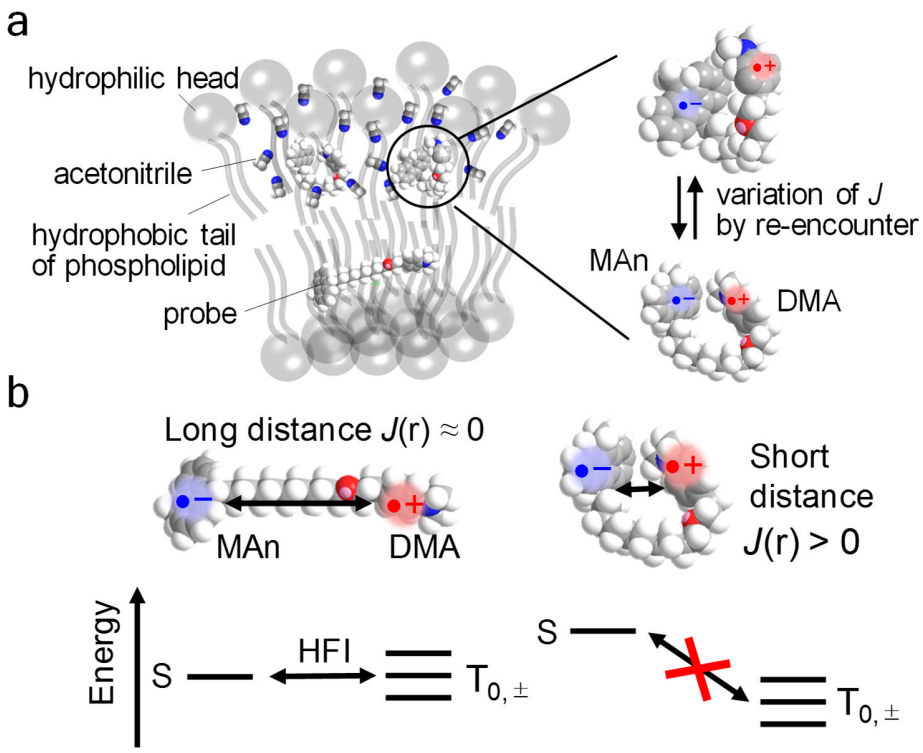

Figure 7. (a) Schematic diagram of probe molecules in lipid bilayer membrane, where acetonitrile molecules are coordinated to hydrophilic groups of lipids. (b) Energy diagram[49] when distance between MAn and DMA is short or long.

In the many aggregates with an average size of 380 nm shown in Figures 3a and S12b-d, MFEs did not occur even though ε values of over 10 were estimated from the peak wavelengths of exciplex emission (Figures 2b and S13). This observation indicates the importance of the mobility of the probe molecules. When the distance between MAn and DMA is sufficiently long, J is negligibly small, therefore the ISC occurs through HFI (Figure 7b).[49] However, as the distance shortens, J increases, and the ISC between S and $T_{0,\pm}$ is hindered. In solution, since the interspin distance of the RIP varies over time, MFEs occur effectively. Meanwhile, when the chain length between the acceptor and donor molecules is short, MFEs are extremely small or absent.[23–25] This situation prevents the RIP from diffusing to an effective distance where J is

negligible. The suppression of mobility is supported not only by MFE but also by the relationship between the intensity and peak energy of exciplex (Figure S18). In addition, it has been demonstrated that the mobility of lipid molecules in curvature membrane is much more limited than in planar membranes from measurements using single-molecule tracking analysis.[3] In regions with high curvatures, such as aggregates, it seems that the increased local viscosity may limit the collision and dissociation between donor and acceptor of the probe molecule. Thus, the MFE imaging could visualize the specific membrane states with adequate polarity and viscosity during the changing of the lipid bilayer state (Figures 5 and 6).

4. CONCLUSIONS

In summary, an MFE-based fluorescence microspectroscopy technique was developed to explore both the local polarity and motional freedom surrounding the probe molecule in the membranes. The vesicle formation during the membrane deformation was selectively visualized through the MFEs, thus allowing the extraction of information on the cellular dynamics at high temporal and spatial resolutions. This MFE-based imaging technique will provide opportunities to investigate molecular interactions and reactions in a broad range of heterogeneous systems, including biological cells and optoelectronic devices.

ASSOCIATED CONTENT

Supporting Information. The following files are available free of charge.

Synthesis procedures of the probe molecule; solvent polarity dependence of exciplex emission; $B_{1/2}$ value of MAn-10-O-2-DMA in butyronitrile; confirmation of membrane formation;

observation of vesicles dissociating from membrane surface; micropolarity in the deformed membranes; fluorescence spectrum of aggregate; confirmation of exciplex emission; photobleaching of bright spots; additional discussion about possible origins of the increase in $B_{1/2}$; the relationship between the intensity and peak energy of exciplex.

AUTHOR INFORMATION

Corresponding Author

* E-mail: tachikawa@port.kobe-u.ac.jp

Notes

The authors declare no competing financial interest.

ACKNOWLEDGMENT

This work was partially supported by JSPS KAKENHI Grant Numbers JP18H01944, JP18H04517, and others, and by Sumitomo Electric Industries Group CSR Foundation.

REFERENCES

(1) Vereb, G.; Szöllosi, J.; Matkó, J.; Nagy, P.; Farkas, T.; Vígh, L.; Mátyus, L.; Waldmann, T. A.; Damjanovich, S. Dynamic, yet Structured: The Cell Membrane Three Decades after the Singer-Nicolson Model. *Proc. Natl. Acad. Sci. U. S. A.* **2003**, *100*, 8053–8058.

(2) Cebecauer, M.; Amaro, M.; Jurkiewicz, P.; Sarmento, M. J.; Šachl, R.; Cwiklik, L.; Hof, M. Membrane Lipid Nanodomains. *Chem. Rev.* **2018**, *118*, 11259–11297.

(3) Kabbani, A. M.; Woodward, X.; Kelly, C. V. Revealing the Effects of Nanoscale Membrane Curvature on Lipid Mobility. *Membranes* **2017**, *7*, 7040060/1-7040060/16.

(4) Hamada, T.; Hirabayashi, Y.; Ohta, T.; Takagi, M. Rhythmic Pore Dynamics in a Shrinking Lipid Vesicle.

Phys. Rev. E **2009**, *80*, 051921/1-051921/7.

(5) Hamada, T.; Hagihara, H.; Morita, M.; Vestergaard, M. C.; Tsujino, Y.; Takagi, M. Physicochemical Profiling of Surfactant-Induced Membrane Dynamics in a Cell-Sized Liposome. *J. Phys. Chem. Lett.* **2012**, *3*, 430–435.

(6) Yoshida, K.; Horii, K.; Fujii, Y.; Nishio, I. Real-Time Observation of Liposome Bursting Induced by Acetonitrile. *ChemPhysChem* **2014**, *15*, 2909–2912.

(7) Yoshida, K.; Mitsumori, R.; Horii, K.; Takashima, A.; Nishio, I. Acetonitrile-Induced Destabilization in Liposomes. *Coloid. Interface.* **2018**, *2*, 2010006/1-2010006/9.

(8) Almgren, M. Mixed Micelles and Other Structures in the Solubilization of Bilayer Lipid Membranes by Surfactants. *Biochim. Biophys. Acta, Biomembr.* **2000**, *1508*, 146–163.

(9) Tanii, H.; Hashimoto, K. Studies on the Mechanism of Acute Toxicity of Nitriles in Mice. *Arch. Toxicol.* **1984**, *55*, 47–54.

(10) Boggild, M. D.; Peck, R. W.; Tomson, C. R. V. Acetonitrile Ingestion: Delayed Onset of Cyanide Poisoning Due to Concurrent Ingestion of Acetone. *Postgrad. Med. J.* **1990**, *66*, 40–41.

(11) Berezin, M. Y.; Lee, H.; Akers, W.; Achilefu, S. Near Infrared Dyes as Lifetime Solvatochromic Probes for Micropolarity Measurements of Biological Systems. *Biophys. J.* **2007**, *93*, 2892–2899.

(12) Gao, J.; Bosco, D. A.; Powers, E. T.; Kelly, J. W. Localized Thermodynamic Coupling between Hydrogen Bonding and Microenvironment Polarity Substantially Stabilizes Proteins. *Nat. Struct. Mol. Biol.* **2009**, *16*, 684–690.

(13) Zhong, D.; Pal, S.; Zewail, A. H. Femtosecond Studies of Protein-DNA Binding and Dynamics: Histone I. *ChemPhysChem* **2001**, *2*, 219–227.

(14) Lichtman, J. W.; Conchello, J.-A. Fluorescence Microscopy. *Nat. Methods* **2005**, *2*, 910–919.

(15) Giuliano, K. A.; Taylor, D. L. Fluorescent-Protein Biosensors: New Tools for Drug Discovery. *Trends Biotechnol.* **1998**, *16*, 135–140.

(16) Axelrod, D. Total Internal Reflection Fluorescence Microscopy in Cell Biology. *Traffic* **2001**, *2*, 764–774.

(17) Signore, G.; Nifosì, R.; Albertazzi, L.; Storti, B.; Bizzarri, R. Polarity-Sensitive Coumarins Tailored to Live Cell Imaging. *J. Am. Chem. Soc.* **2010**, *132*, 1276–1288.

(18) Someya, Y.; Yui, H. Fluorescence Lifetime Probe for Solvent Microviscosity Utilizing Anilinonaphthalene Sulfonate. *Anal. Chem.* **2010**, *82*, 5470–5476.

(19) Kusube, M.; Matsuki, H.; Kaneshina, S. Effect of Pressure on the Prodan Fluorescence in Bilayer Membranes of Phospholipids with Varying Acyl Chain Lengths. *Coll. Surf. B* **2005**, *42*, 79–88.

(20) Pal, K.; Kattnig, D. R.; Grampp, G.; Landgraf, S. Experimental Observation of Preferential Solvation on a Radical Ion Pair Using MARY Spectroscopy. *Phys. Chem. Chem. Phys.* **2012**, *14*, 3155–3161.

(21) Richert, S.; Rosspeintner, A.; Landgraf, S.; Grampp, G.; Vauthey, E.; Kattnig, D. R. Time-Resolved Magnetic Field Effects Distinguish Loose Ion Pairs from Exciplexes. *J. Am. Chem. Soc.* **2013**, *135*, 15144–15152.

(22) Pal, K.; Grampp, G.; Kattnig, D. R. Solvation Dynamics of a Radical Ion Pair in Micro-Heterogeneous Binary Solvents: A Semi-Quantitative Study Utilizing MARY Line-Broadening Experiments. *ChemPhysChem* **2013**, *14*, 3389–3399.

(23) Hoang, H. M.; Pham, V. T. B.; Grampp, G.; Kattnig, D. R. Magnetic Field-Sensitive Radical Pair Dynamics in Polymethylene Ether-Bridged Donor–Acceptor Systems. *ACS Omega* **2018**, *3*, 10296–10305.

(24) De, R.; Fujiwara, Y.; Zhang, B.; Tanimoto, Y. Magnetic Field Effect on the Intramolecular Exciplex Fluorescence of Chain-Linked Pyrene/N,N-Dimethylaniline Systems. *Bull. Chem. Soc. Jpn.* **2000**, *73*, 1573–1580.

(25) H. Cao, Y. Fujiwara, T. Haino, Y. Fukuzawa, C. Tung, Y. T. Magnetic Field Effects on Intramolecular Exciplex Fluorescence of Chain-Linked Phenanthrene and N,N-Dimethylaniline: Influence of Chain Length, Solvent, and Temperature. *Bull. Chem. Soc. Jpn.* **1996**, *69*, 2801–2813.

(26) Bhattacharyya, K.; Chowdhury, M. Environmental and Magnetic Field Effects on Exciplex and Twisted Charge Transfer Emission. *Chem. Rev.* **1993**, *93*, 507–535.

(27) Nath, D. N.; Chowdhury, M. Effect of Variation of Dielectric Constant on the Magnetic Field Modulation of Exciplex Luminescence. *Pramana* **1990**, *34*, 51–66.

(28) H. Staerk, H. G. Busmann, W. Kuhnle, A. W. Solvent Effects on the Magnetic-Field-Dependent Reaction Yields of Photogenerated Radical Ion Pairs. *Chem. Phys. Lett.* **1989**, *155*, 603–608.

(29) N. Kh. Petrov, A. I. Shushin, E. L. F. Solvent Effect on Magnetic Field Modulation of Exciplex Fluorescence in Polar Solutions. *Chem. Phys. Lett.* **1981**, *82*, 339–343.

(30) Steiner, U. E.; Ulrich, T. Magnetic Field Effects in Chemical Kinetics and Related Phenomena. *Chem. Rev.* **1989**, *89*, 51–147.

(31) Werner, U.; Staerk, H. Magnetic Field Effect in the Recombination Reaction of Radical Ion Pairs: Dependence on Solvent Dielectric Constant. *J. Phys. Chem.* **1995**, *99*, 248–254.

(32) Timmel, C. R.; Till, U.; Brocklehurst, B.; McLauchlan, K. A.; Hore, P. J. Effects of Weak Magnetic Fields on Free Radical Recombination Reactions. *Mol. Phys.* **1998**, *95*, 71–89.

(33) Iwasaki, Y.; Maeda, K.; Murai, H. Time-Domain Observation of External Magnetic Field Effects on the Delayed Fluorescence of N,N,N',N-Tetramethyl-m-Phenylenediamine in Alcoholic Solution. *J. Phys. Chem. A* **2001**, *105*, 2961–2966.

(34) Aich, S.; Basu, S. Magnetic Field Effect : A Tool for Identification of Spin State in a Photoinduced Electron-Transfer Reaction. *J. Phys. Chem. A* **1998**, *102*, 722–729.

(35) Cao, H.; Miyata, K.; Tamura, T.; Fujiwara, Y.; Katsuki, A.; Tung, C. H.; Tanimoto, Y. Effects of High Magnetic Field on the Intramolecular Exciplex Fluorescence of Chain-Linked Phenanthrene and Dimethylaniline. *J. Phys. Chem. A* **1997**, *101*, 407–411.

(36) Tanimoto, Y.; Hasegawa, K.; Okada, N.; Itoh, M.; Iwai, K.; Sugioka, K.; Takemura, F.; Nakagaki, R.; Nagakura, S. Magnetic Field Effects on the Intra- and Intermolecular Exciplex Fluorescence of Phenanthrene and Dimethylaniline. *J. Phys. Chem.* **1989**, *93*, 3586–3594.

(37) Beardmore, J. P.; Antill, L. M.; Woodward, J. R. Optical Absorption and Magnetic Field Effect Based Imaging of Transient Radicals. *Angew. Chem.* **2015**, *54*, 8494–8497.

(38) Antill, L. M.; Beardmore, J. P.; Woodward, J. R. Time-Resolved Optical Absorption Microspectroscopy of Magnetic Field Sensitive Flavin Photochemistry. *Rev. Sci. Instrum.* **2018**, *89*.

(39) Lee, H.; Yang, N.; Cohen, A. E. Mapping Nanomagnetic Fields Using a Radical Pair Reaction. *Nano Lett.* **2011**, *11*, 5367–5372.

(40) Yang, N.; Cohen, A. E. Optical Imaging through Scattering Media via Magnetically Modulated Fluorescence: Erratum. *Opt. Express* **2011**, *19*, 5397.

(41) Nakayama, K.; Tachikawa, T.; Majima, T. Spatial Control of Protein Binding on Lipid Bimembrane Using Photoeliminative Linker. *Langmuir* **2008**, *24*, 6425–6428.

(42) Richert, S.; Rosspeintner, A.; Landgraf, S.; Grampp, G.; Vauthey, E.; Kattnig, D. R. Time-Resolved Magnetic Field Effects Distinguish Loose Ion Pairs from Exciplexes. *J. Am. Chem. Soc.* **2013**, *135*, 15144–15152.

(43) Hoang, H. M.; Van Pham, T. B.; Grampp, G.; Kattnig, D. R. Exciplexes versus Loose Ion Pairs: How Does the Driving Force Impact the Initial Product Ratio of Photoinduced Charge Separation Reactions? *J. Phys. Chem. Lett.* **2014**, *5*, 3188–3194.

(44) Lippert, E. Z. The Solvent Effect on the Spectral Shift. *Naturforsch.* **1955**, *10a*, 541.

(45) Mataga, N.; Kaifu, Y.; Koizumi, M. The Solvent Effect on Fluorescence Spectrum, Change of Solute-Solvent Interaction during the Lifetime of Excited Solute Molecule. *Bull. Chem. Soc. Jpn.* **1955**, *28*, 690–691.

(46) Kattnig, D. R.; Rosspeintner, A.; Grampp, G. Magnetic Field Effects on Exciplex-Forming Systems: The Effect on the Locally Excited Fluorophore and Its Dependence on Free Energy. *Phys. Chem. Chem. Phys.* **2011**, *13*, 3446–3460.

(47) McMahon, H. T.; Gallop, J. L. Membrane Curvature and Mechanisms of Dynamic Cell Membrane Remodelling. *Nature* **2005**, *438*, 590–596.

(48) Miura, T.; Maeda, K.; Arai, T. The Spin Mixing Process of a Radical Pair in Low Magnetic Field Observed by Transient Absorption Detected Nanosecond Pulsed Magnetic Field Effect. *J. Phys. Chem. A* **2006**, *110*, 4151–4156.

(49) Kobori, Y.; Sekiguchi, S.; Akiyama, K.; Tero-Kubota, S. Chemically Induced Dynamic Electron Polarization Study on the Mechanism of Exchange Interaction in Radical Ion Pairs Generated by Photoinduced Electron Transfer Reactions. *J. Phys. Chem. A* **1999**, *103*, 5416–5424.